

Three-Dimensional Bulk Electronic Structures of $\text{Ca}_{1.5}\text{Sr}_{0.5}\text{RuO}_4$ Studied by Soft X-ray Angle-Resolved Photoemission

M. Uruma,¹ A. Sekiyama,¹ H. Fujiwara,¹ M. Yano,¹ H. Fujita,¹
S. Imada,¹ T. Muro,² I. A. Nekrasov,³ Y. Maeno,⁴ and S. Suga¹

¹*Division of Materials Physics, Graduate School of Engineering Science,
Osaka University, Toyonaka, Osaka 560-8531, Japan*

²*Japan Synchrotron Radiation Research Institute, SPring-8, Mikazuki, Hyogo 679-5198, Japan*

³*Institute of Electrophysics, Russian Academy of Sciences-Ural Division, 626041 Yekaterinburg, GSP-170, Russia*

⁴*Department of Physics, Kyoto University, Kyoto 606-8502, Japan*

(Dated: November 25, 2021)

We report on experimental data of the three-dimensional bulk Fermi surfaces of the layered strongly correlated $\text{Ca}_{1.5}\text{Sr}_{0.5}\text{RuO}_4$ system. The measurements have been performed by means of $h\nu$ -dependent bulk-sensitive soft x-ray angle-resolved photoemission technique. Our experimental data evinces the bulk Fermi surface topology at $k_z \sim 0$ to be qualitatively different from the one observed by surface-sensitive low-energy ARPES. Furthermore, stronger k_z dispersion of the circle-like γ Fermi surface sheet is observed compared with Sr_2RuO_4 . Thus in the paramagnetic metal phase, $\text{Ca}_{1.5}\text{Sr}_{0.5}\text{RuO}_4$ compound is found to have rather three-dimensional electronic structure.

PACS numbers: 79.60.-i, 71.20.-b, 71.30.+h

Strongly correlated transition metal oxides are widely studied because of a variety of such intriguing phenomena as (high-temperature) anisotropic superconductivity, Mott transition, magnetic and/or orbital ordering, and large mass enhancement. Among them, the single-layered perovskite $\text{Ca}_{2-x}\text{Sr}_x\text{RuO}_4$ is particularly interesting, since it shows various phases as functions of temperature and x [1, 2]. By substituting Sr^{2+} -ions for isovalent Ca^{2+} -ions, the unconventional superconductivity takes place below ~ 1.5 K for $x = 2$. A paramagnetically metallic behavior with strong electron correlation is seen in a wide temperature region for $0.5 < x < 2$. The system shows a paramagnetic metal to “magnetic” metal transition at 10 K, for $0.2 < x < 0.5$, and eventually becomes a Mott insulator for $x < 0.2$. At the Sr concentration of $x = 0.5$, it is furthermore known that the effective mass diverges below 10 K although the system does not undergo a Mott transition [2, 3]. These phenomena are thought to originate not only from the enhanced electron correlation by the rotation of the RuO_6 octahedra (Ru-O-Ru bonds are bent from ideal ones), but also from the reduction of orbital degree of freedom by a Jahn-Teller distortion [4, 5, 6, 7] and/or a Ru 4d spin-orbit interaction. Indeed, a (partial) Ru 4d orbital-ordering has been reported (proposed) for $x = 0$ [8] ($0.2 < x < 0.5$ [3, 4]).

Angle-resolved photoemission (ARPES) is a very powerful tool to evince band dispersions and Fermi surface (FS) topology. So far, several low- $h\nu$ ARPES experiments were performed for $\text{Ca}_{2-x}\text{Sr}_x\text{RuO}_4$ [9, 10, 11, 12]. However, it is known that low-energy photoemission is surface-sensitive and often provides spectral shapes which are not consistent with bulk electronic structures [13, 14, 15, 16]. Meanwhile, it has been demonstrated that high- $h\nu$ ARPES with use of the soft x-ray can reveal detailed band dispersions of the bulk electronic

states [17, 18, 19]. In addition, by virtue of the longer mean free path of higher kinetic energy photoelectrons the high-energy $h\nu$ -dependent ARPES can probe electronic structures of three-dimensional compounds with better-resolved k_z dispersion (k_z - momentum component perpendicular to the cleaved sample surface) [19, 20, 21].

High quality single crystal of $\text{Ca}_{1.5}\text{Sr}_{0.5}\text{RuO}_4$ ($x = 0.5$), which was grown by the floating zone method [22], was used for the measurement. All ARPES measurements were performed at BL25SU in SPring-8 [23]. The high-energy ($h\nu = 708$ eV) and low-energy ($h\nu = 362$ eV) soft x-ray ARPES and FS mapping were carried out for the $k_z \sim 0$ plane. In addition, $h\nu$ dependent ($h\nu = 650\text{--}730$ eV) ARPES for the $k_x=0$ plane FS mapping was done with the energy step of 5 eV. The base pressure was about 4×10^{-8} Pa. The (001) clean surface was obtained by cleaving the sample *in situ* at the measuring temperature of 20 K. The overall energy resolution was set to 200 meV. The angular resolution was $\pm 0.15^\circ$ ($\pm 0.25^\circ$) for the parallel (perpendicular) direction to the analyzer slit.

Figure 1 shows the $h\nu$ dependence of the angle-integrated Sr 3d core-level photoemission (PES) spectra of $\text{Ca}_{1.5}\text{Sr}_{0.5}\text{RuO}_4$. To our understanding these spectra contain three components corresponding to the contributions from the top-most SrCaO surface layer (S1), the second SrCaO surface layer (S2) located just below the top RuO_2 layer, and the bulk layers [17]. The intensity of the S1 and S2 shoulders is observed to be remarkably stronger for $h\nu = 362$ eV (blue curve) than for $h\nu = 708$ eV (red curve). To estimate the bulk contribution to the spectra we did line-shape analysis in the same manner as in Ref. [17]. The bulk contribution is estimated to be 55% (39%) in the Sr 3d spectra at $h\nu = 708$ (362) eV. These values are close to the ones evaluated for the given lattice constants and the calculated photoelectron

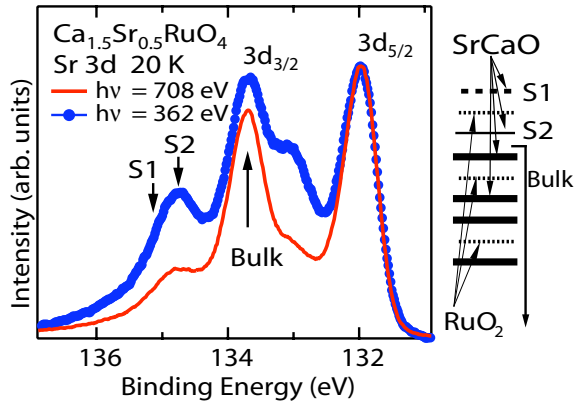


FIG. 1: (color online) Left panel: $h\nu$ dependence of the Sr 3d core-level PES spectra of $\text{Ca}_{1.5}\text{Sr}_{0.5}\text{RuO}_4$ with the energy resolution of 200 meV. The spectra are normalized at the $3d_{5/2}$ main peak. The dots with line and solid line correspond to $h\nu = 362$ eV and 708 eV. Right panel: schematic picture of atomic layers. Strong surface contribution is expected from top-most SrCaO surface layer (S1) and the second SrCaO surface layer (S2) placed just below the top RuO_2 layer.

mean free path λ [20]. Then, the bulk contribution in the valence-band is found to be $\sim 65\%$ at $h\nu = 708$ eV and $\sim 50\%$ at $h\nu = 362$ eV, manifesting that the 708 eV-PES mainly probes the bulk valence states.

In the following, we show the FSs derived from the 708 eV- and 362 eV-ARPES spectral intensity integrated from -0.1 to 0.1 eV with respect to the Fermi level (E_F) (Figs. 2 (a) and (b)). These results are obtained from energy distribution curves (EDCs) (Figs. 2 (e)-(h)) in the paramagnetic metal phase at 20 K. Figures 2(a) and 2(b) display raw data and Figs. 2(c) and 2(d) summarize remarkable features (see captions). We have obtained k_F (E_F -crossing points in a reciprocal space) from both EDCs and momentum distribution curves (MDCs: not shown here) as plotted in Figs. 2 (a) and (b) with a two-dimensional cubic symmetry BZ. Although the true BZ of $\text{Ca}_{1.5}\text{Sr}_{0.5}\text{RuO}_4$ is $\sqrt{2} \times \sqrt{2}$ folded because of the rotation RuO_6 octahedra along the c -axis ($\sim 12^\circ$ [5]), we use the size of BZ and notations for high symmetry directions of the Sr_2RuO_4 crystal structure. EDCs in Figs. 2(e)-(h) correspond to shaded areas in Figs. 2(c) and (d). As shown in Fig. 2(e), two branches (β and γ) located at 0.5 eV at $(0,0)$ approach and cross E_F between $(0,0)$ and $(0,\pi)$ in the 708 eV-ARPES spectra. In the 362 eV-ARPES spectra in Fig. 2(g), we observed one additional branch between these two branches crossing E_F . Considering that the 362 eV-ARPES is more surface sensitive, we attribute this additional branch (which spectral weight is noticeably suppressed in the 708 eV-ARPES spectra) to be resulting from the surface band different from the bulk one. Along the $(\pi,0)$ - (π,π) direction, we have likewise found that two branches cross E_F in the 708 eV-ARPES spectra (Fig. 2(f)), whereas three

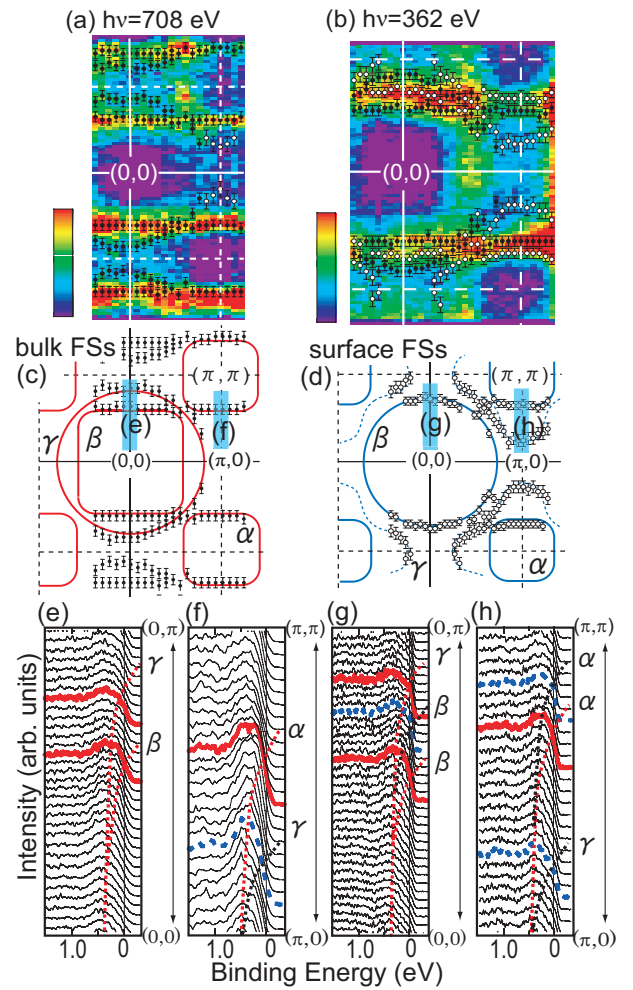


FIG. 2: (color online) (a),(b) Experimental $\text{Ca}_{1.5}\text{Sr}_{0.5}\text{RuO}_4$ FS intensity map at $k_z \sim 0$ obtained by the 708 eV-ARPES and 362 eV-ARPES, respectively. The filled and empty circles represent the experimental k_F values for the bulk and surface as discussed in the text. (c),(d) Schematic FS (red, blue lines) with respect to (a),(b). The surface FS observed in (a) is not drawn in (c) and the bulk FSs revealed in (b) are not shown in (d) for simplicity. The blue dashed line in (d) reproduces the low-energy ARPES data of Ref. [11]. (e),(f): 708 eV-ARPES spectra along $(0,0)$ - $(0,\pi)$ and $(\pi,0)$ - (π,π) directions within shaded areas in (c),(d). (g),(h): 362 eV-ARPES data along the same direction as (e),(f). Red dashed and black dashed lines are experimental band dispersions for bulk and surface, which are evaluated by the momentum distribution curves (MDCs). The red-bold and blue-dashed lines in (e)-(h) correspond to bulk and surface spectra at k_F . The BZ corresponds to ideal two-dimensional cubic lattice in which the effect of RuO_6 rotation is not taken into account.

branches cross E_F in the 362 eV-ARPES spectra (Fig. 2(h)). Hence essentially dissimilar electronic structures and Fermi surface topology (at $k_z \sim 0$) between the bulk and surface states for this “quasi” two-dimensional electron system are demonstrated.

As shown in Figs. 2(a) and 2(c) by 708 eV-ARPES

measurements, we have found three bulk FS sheets for $\text{Ca}_{1.5}\text{Sr}_{0.5}\text{RuO}_4$, namely, one hole-like square-shaped α sheet centered at (π, π) , one electron-like square-shaped β sheet and one electron-like circle-shaped γ sheet both centered at $(0, 0)$. Our FS topology observed for $k_z \sim 0$ plane is thus very similar to that of bulk sensitive experimental data for Sr_2RuO_4 and $\text{Ca}_{0.2}\text{Sr}_{1.8}\text{RuO}_4$ [17]. If one assume that orbital character for the FS sheets remains the same as for Sr_2RuO_4 , then α and β sheets should correspond mainly to the Ru $4d_{yz/zx}$ orbitals whereas the γ sheet has mainly the Ru $4d_{xy}$ character. Possible effects of the BZ folding caused by the RuO_6 rotation [24] are not seen (or negligibly weak) in our results in strong contrast to the low-energy ARPES result for Sr_2RhO_4 and Sr_2RuO_4 surface [10, 25]. The reason for the absence of the BZ folding effect is, however, not clear at present.

On the other hand, the 362 eV-ARPES results (Fig. 2(b)) clearly reveal three surface FS sheets (open circles) distinguished from the bulk FS sheets. While the shape of the surface α sheet is rather similar to the bulk one as recognized by comparing Figs. 2(c) and (d), the electron-like surface β sheet is much more circle-like compared to the bulk β sheet. Furthermore, the FS topology of the γ sheet is qualitatively different between the bulk in Fig. 2(c) and surface in Fig. 2(d). The hole-like surface γ sheet observed here well traces the result of the low-energy ARPES at $h\nu = 32$ eV [11] reproduced by the dashed curves in Fig. 2(d). The scanning tunneling microscopy (STM) measurement of Sr_2RuO_4 has shown a surface reconstruction [26]. Except for this report no surface reconstruction has been reported for $\text{Ca}_{2-x}\text{Sr}_x\text{RuO}_4$. It has been believed that the bulk FSs can be detected even by the surface-sensitive low-energy ARPES for $\text{Ca}_{2-x}\text{Sr}_x\text{RuO}_4$ since the RuO_6 rotation angle indicates similar crystal structures between the bulk ($\sim 12^\circ$) and surface ($\sim 11^\circ$) [11]. However, our result evinces that the surface FS topology is noticeably different from the bulk.

Below we discuss experimental data on interlayer coherent electron hopping or in other words k_z dispersion of the FS observed by our bulk sensitive $h\nu$ dependent ARPES measurements. A nearly free photoelectron model calculation with the inner potential of 9 eV identifies Γ and Z points of a tetragonal BZ with $h\nu$ s of 712 and 664 eV in our experiment [27].

Figure 3(a) shows the results of $h\nu$ -dependent ARPES for $\text{Ca}_{1.5}\text{Sr}_{0.5}\text{RuO}_4$, representing the k_z dispersion of the β and the γ FS sheets. The γ FS sheet is found to have significant k_z dependence reflecting stronger three-dimensionality of the $\text{Ca}_{1.5}\text{Sr}_{0.5}\text{RuO}_4$ electronic structure. This is in strong contrast to results of quantum oscillation measurements for Sr_2RuO_4 showing negligible k_z dependence for the γ sheet [29, 31]. On the other hand, our result has revealed much weaker k_z dependence of the β FS sheet compared with that of the γ FS sheet. Indeed, a ratio of k_F between the minimum and maxi-

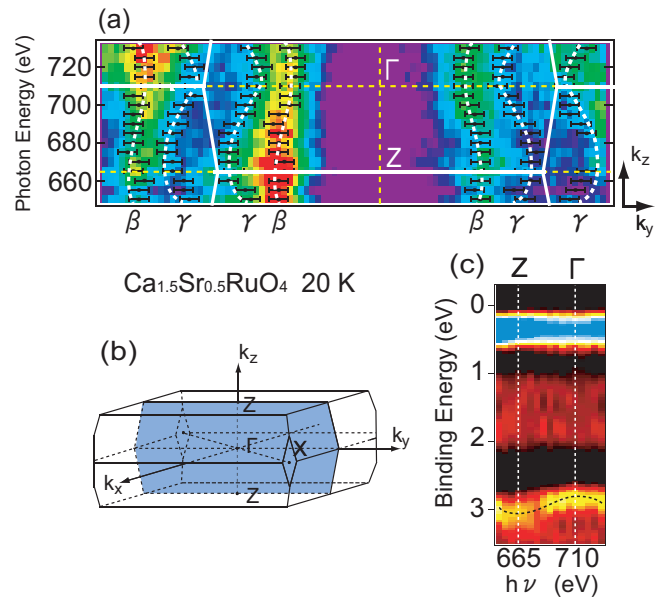


FIG. 3: (color online) (a) Obtained by $h\nu$ -dependent ARPES measurements intensity map integrated over $E_F \pm 0.1$ eV for $\text{Ca}_{1.5}\text{Sr}_{0.5}\text{RuO}_4$ in the $k_x=0$ plane. The black dots with the error bars represent experimental k_F values. The white solid lines represent part of tetragonal BZ boundaries shown in (b). (c) Second derivative of the EDCs along the Γ - Z direction. The black dashed curve near 3 eV is the guide to the eye.

mum along the Γ - Z direction has been estimated to be ~ 0.9 for the β sheet whereas for the γ sheet it is ~ 0.8 . So far it has been considered that the electronic structures and FSs of such single-layered transition metal oxides as $\text{Ca}_{2-x}\text{Sr}_x\text{RuO}_4$ are highly two-dimensional. However, those for $\text{Ca}_{1.5}\text{Sr}_{0.5}\text{RuO}_4$ are found to be more three-dimensional than Sr_2RuO_4 from our experiments.

As shown in Fig. 3(c), the spectral weight near 3 eV in the ARPES data disperses clearly as a function of $h\nu$. Its bottom (top) is located at Z (Γ). This dispersion is qualitatively consistent with results of the band-structure calculation for Sr_2RuO_4 along the Γ - Z (k_z) direction [28, 29, 30]. However there seems to be also non-dispersive contribution at 3 eV. These k -independent spectral structure observed at ~ 1 -2 and 3 eV can be presumably identified as the part of the Ru $4d(t_{2g})$ lower Hubbard band similar to our recent LDA+DMFT(QMC) results for Sr_2RuO_4 [30]. Namely, correlations in $\text{Ca}_{1.5}\text{Sr}_{0.5}\text{RuO}_4$ can be enhanced due to distortion in comparison with Sr_2RuO_4 .

Since the bulk FS topology of $\text{Ca}_{1.5}\text{Sr}_{0.5}\text{RuO}_4$ at $k_z \sim 0$ observed by us is similar to Sr_2RuO_4 one can expect the orbital characters of the relatively large γ and small β sheets to be of the Ru $4d_{xy}$ and $4d_{yz/zx}$ symmetries, respectively. In that way our results seem to contradict with theoretical expectation where strong k_z dependence is usually expected for the Ru $4d_{yz/zx}$ -derived bands rather than for the Ru $4d_{xy}$ band [28, 29, 30].

One possible explanation of our ARPES results is that the characters of the β and γ FS sheets are interchanged with each other compared with those for Sr_2RuO_4 . Our LDA (local density approximation) band-structure calculation [32] as well as that in Ref. [24] predict such a scenario as the smallest electron-like two-dimensional FS sheet originates from the Ru $4d_{xy}$ band. But this FS sheet is caused by doubling of the lattice in $\text{Ca}_{1.5}\text{Sr}_{0.5}\text{RuO}_4$. As mentioned above in our ARPES results, bands coming from folding are negligibly weak. We have surveyed not only the reciprocal space shown in Figs. 2 and 3 but also the $k_x - k_y$ plane at $h\nu = 650$ eV (not shown here) covering first and second BZs by ARPES, therefore the absence of these hole-like FS sheets is thought to be intrinsic in this experiment for $\text{Ca}_{1.5}\text{Sr}_{0.5}\text{RuO}_4$ system.

Another scenario of rather strong k_z dependence of the γ sheet can be by the effect of the RuO_6 rotation within the conducting plane. By virtue of the rotation, there appears small but finite σ -bonding between the Ru $4d_{xy}$ and the O $2p_{x/y}$ orbitals. So the situation becomes similar to high- T_C cuprate La_2CuO_4 [33], where it was shown that such σ -bonding leads to essentially three-dimensional $x^2 - y^2$ -symmetry Wannier function. For $\text{Ca}_{1.5}\text{Sr}_{0.5}\text{RuO}_4$ this effect is weaker than for La_2CuO_4 . Nevertheless Ru $4d_{xy}$ -derived band in the distorted crystal structure can form rather three-dimensional γ sheet. Also one should mention here that more two-dimensional square-shaped β sheet has stronger nesting instability as observed in Sr_2RuO_4 and $\text{Ca}_{0.2}\text{Sr}_{1.8}\text{RuO}_4$ [17, 34]. Thus the Ru $4d_{yz/zx}$ orbital ordering scenario within the magnetic metal phase for $0.2 < x < 0.5$ [4] is possible.

To summarize, we have observed three-dimensional Fermi surfaces of $\text{Ca}_{1.5}\text{Sr}_{0.5}\text{RuO}_4$ in the paramagnetic metal phase at 20 K by applying bulk sensitive soft x-ray $h\nu$ -dependent ARPES technique. We have revealed the genuine bulk electronic structures which are different from surface sensitive data for this material. FS topology in the $k_z \sim 0$ plane is observed to be qualitatively similar with bulk FS of Sr_2RuO_4 . However remarkable k_z dependence of the γ FS sheet have proved $\text{Ca}_{1.5}\text{Sr}_{0.5}\text{RuO}_4$ to have more three-dimensional electronic structure than Sr_2RuO_4 .

We are grateful to H. Higashimichi, G. Funabashi, and T. Nakamura for supporting the experiments. This work was supported by a Grant-in-Aid for Scientific Research (15GS0213, 1814007, 18684015) and the 21st COE program (G18) of the Japan Society for the Promotion of Science and MEXT. This work was also supported by

Hyogo Science and Technology Association. The ARPES was performed at SPring-8 under the approval of JASRI (2006A1169, 2007A1005). IN thanks RFFI grants 08-02-00021, 08-02-00712, 08-02-91200, 06-02-90537, travel grant of UB RAS and grant of President of Russia MK-2242.2007.2.

-
- [1] Y. Maeno *et al.*, Nature **372**, 532 (1994).
 - [2] S. Nakatsuji and Y. Maeno, Phys. Rev. Lett. **84**, 2666 (2000).
 - [3] S. Nakatsuji *et al.*, J. Phys. Rev. Lett. **90**, 137202 (2003).
 - [4] V. I. Anisimov *et al.*, Eur. Phys. J. B **25**, 191 (2002).
 - [5] O. Friedt *et al.*, Phys. Rev. B **63**, 174432 (2001).
 - [6] T. Mizokawa *et al.*, Phys. Rev. Lett. **87**, 077202 (2001).
 - [7] T. Hotta and E. Dagotto, Phys. Rev. Lett. **88**, 017201 (2001).
 - [8] I. Zegkinoglou *et al.*, Phys. Rev. Lett. **95**, 136401 (2005).
 - [9] A. Damascelli *et al.*, Phys. Rev. Lett. **85**, 5194 (2000).
 - [10] K. M. Shen *et al.*, Phys. Rev. B **64**, 180502(R) (2001).
 - [11] S.-C. Wang *et al.*, Phys. Rev. Lett. **93**, 177007 (2004).
 - [12] J. Zhang *et al.*, Phys. Rev. Lett. **96**, 066401 (2006).
 - [13] A. Sekiyama *et al.*, Nature (London) **403**, 396 (2000).
 - [14] A. Sekiyama *et al.*, J. Phys. Soc. Jpn. **69**, 2771 (2000).
 - [15] A. Sekiyama *et al.*, Phys. Rev. Lett. **93**, 156402 (2004).
 - [16] S. Suga *et al.*, J. Phys. Soc. Jpn. **74**, 2880 (2005).
 - [17] A. Sekiyama *et al.*, Phys. Rev. B **70**, 060506(R) (2004).
 - [18] S. Suga *et al.*, Phys. Rev. B **70**, 155106 (2004).
 - [19] M. Yano *et al.*, Phys. Rev. Lett. **98**, 036405 (2007).
 - [20] S. Tanuma, C. J. Powell, and D. R. Penn, J. Vac. Sci. Technol. A **8**, 2213 (1990).
 - [21] H. Wadati *et al.*, Phys. Rev. B **71**, 035108 (2005).
 - [22] S. Nakatsuji and Y. Maeno, J. Solid State Chem. **156**, 26 (2001).
 - [23] Y. Saitoh *et al.*, Rev. Sci. Instrum. **71**, 3254 (2000).
 - [24] E. Ko, B. J. Kim, C. Kim, and H. J. Choi, Phys. Rev. Lett. **98**, 226401 (2007).
 - [25] B. J. Kim *et al.*, Phys. Rev. Lett. **97**, 106401 (2006).
 - [26] R. Matzdorf *et al.*, Science **289**, 746 (2000).
 - [27] We have measured the ARPES spectra with the polar angles near 0° and at the photon incident angle of 45° .
 - [28] T. Oguchi, Phys. Rev. B **51**, 1385 (1995).
 - [29] Y. Yoshida *et al.*, J. Phys. Soc. Jpn. **67**, 1677 (1998).
 - [30] Z. V. Pchelkina *et al.*, Phys. Rev. B **75**, 035122 (2007).
 - [31] A. P. Mackenzie *et al.*, Phys. Rev. Lett. **76**, 3786 (1996).
 - [32] We perform TB-LMTO [O.K. Andersen and O. Jepsen Phys. Rev. Lett. **53**, 2571 (1984)] calculations with following NMTO [O.K. Andersen and T. Saha-Dasgupta, Phys. Rev. B **62**, R16219 (2000)] analysis.
 - [33] E. Pavarini *et al.*, Phys. Rev. Lett. **87**, 047003 (2001).
 - [34] Y. Sidis *et al.*, Phys. Rev. Lett. **83**, 3320 (1999).